

Temperature dependence of the optical properties of VO₂ deposited on sapphire with different orientations

M. Nazari,¹ Y. Zhao,² V. V. Kuryatkov,² Z. Y. Fan,² A. A. Bernussi,² and M. Holtz¹

¹*Department of Physics and Nano Tech Center, Texas Tech University, Lubbock, Texas 79409, USA*

²*Department of Electrical and Computer Engineering and Nano Tech Center, Texas Tech University, Lubbock, Texas 79409, USA*

(Received 14 August 2012; published 31 January 2013)

Spectroscopic ellipsometry studies are reported for vanadium dioxide grown on *c*-, *m*-, and *r*-plane sapphire substrates. The crystallographic orientation of the VO₂ depends strongly on the substrate, producing diverse strains in the layers which affect the interband transition energies and the phase transition temperatures. These structural differences correlate with distinct variations of the optical transitions observed in the ellipsometry results. For the *m*- and *r*-plane substrates, the VO₂ appears to transform abruptly from the monoclinic phase to the rutile *R* structure as temperature is increased. In contrast, VO₂ deposited on *c*-plane sapphire exhibits a sluggish transformation. For the *m*-plane sample, the energy gap collapses over a narrow temperature range. For the *c*-plane case, a broad temperature range is obtained between the onset and completion of the transformation. Raman studies of the vibrational structure show that internal stresses due to expansion and contraction across the phase transitions impacts the observed phonon energies.

DOI: [10.1103/PhysRevB.87.035142](https://doi.org/10.1103/PhysRevB.87.035142)

PACS number(s): 71.30.+h, 78.66.Jg, 78.30.Am, 73.22.-f

I. INTRODUCTION

Vanadium dioxide is receiving significant attention due to the well-known metal-insulator phase transition (MIT) at temperature $T_{\text{MIT}} = 68^\circ\text{C}$.¹ The transformation is accompanied by a structural phase transition (SPT) from low-temperature monoclinic (M_1) symmetry, in which the material is characterized as a narrow gap insulator, to high-temperature tetragonal rutile (*R*), in which the material is metallic.^{2,3} The V-V chains, which lie along the a_m axis in the M_1 phase (and corresponding C_R axis in the *R* phase), form a zigzag chain at low T . At high T the V-V pairs straighten and shift to form a linear chain along C_R comprised of equidistant V⁴⁺ ions.

Several factors known to affect T_{MIT} of VO₂ include nanocrystal domain size^{4,5} and stress.⁶ Recent investigations of the effect of stress on VO₂ have resulted in new understanding of the material phase diagram.⁷⁻¹² Stress along the M_1 (011) crystal axis, corresponding to $(110)_R$,¹³ has been shown to induce a phase transition from the M_1 phase to M_2 , in which alternating V chains pair without twisting, while the others twist without pairing.^{14,15} Gu *et al.*¹¹ showed that the M_2 phase is induced by a variety of stresses, and Tselev *et al.*¹⁶ used the Landau-Ginzburg model for examining how stress affects the M_1 - M_2 -*R* phase diagram. Recent work on single crystal microbeams of VO₂ deposited on oxidized silicon and then transferred on flexible polycarbonate substrate has revealed the transformation from M_1 to M_2 may be gradual, resulting in an additional phase of VO₂ with triclinic symmetry.¹² The effect of substrate-induced strain has also been shown to influence T_{MIT} in VO₂ thin films.^{6,17} Since the majority of potential applications for VO₂ rely on thin films, we investigate the role of substrate-induced strains for situations both favoring and inhibiting the formation of M_2 as T_{MIT} is approached. Strain in these samples arises from lattice-constant mismatches with the substrate and thermal stresses due to the different expansion coefficients of VO₂ and sapphire.

Despite its usefulness for examining the electronic band structure of states principally related to conduction, there are

few spectroscopic ellipsometry (SE) studies of VO₂ and the band structure of this material is not fully established.^{2, 18-21} The low symmetry of VO₂ makes SE measurements challenging to model and interpret. Generally, this is less of an issue in thin films since they are composed of polycrystalline domains having a distribution of orientations which result in measured properties corresponding to isotropic conditions. In this paper we report SE studies of VO₂ deposited on sapphire having different crystal orientations, denoted *c*, *m*, and *r* plane (herein samples *c*, *m*, and *r*). Under identical deposition conditions, described previously along with extensive characterization,²² the sapphire influences the VO₂ orientation. For deposition on *c*-plane sapphire, the VO₂ is predominantly oriented with the V-V chains of the *R* phase in the plane of the sapphire. In contrast, the *m* and *r* samples have the C_R axis directed out of (but not normal to) the sapphire substrate plane. This set of samples corresponds to thin films for which we anticipate compressive strain along the C_R axis in *m* and *r*, and tensile strain along C_R in sample *c*.

The values obtained for T_{MIT} based on our ellipsometry measurements, described below, are 72 ± 2 , 63 ± 2 , and $62 \pm 2^\circ\text{C}$ for the *c*, *m*, and *r* samples, respectively. These T_{MIT} values agree with our prior resistivity (ρ) measurements²² and are all noticeably different from the accepted T_{MIT} for bulk VO₂. Our results thus corroborate the presence of tensile C_R strain in sample *c*, and compressive strain in both *m* and *r*.⁶ Upon cooling sample *c*, differences in the thermal expansion coefficients of sapphire and VO₂ will produce tensile strain in C_R , thereby raising T_{MIT} . Upon cooling the *m* and *r* samples, the substrate will again induce tensile stress in the VO₂ plane of the growth, for which the crystal orientation results in compressive strain in the C_R direction thereby reducing T_{MIT} . We estimate the strain magnitudes to be $\sim 0.1\%$ at room temperature,⁶ in good agreement with our estimates based on published thermal expansion coefficient of VO₂²³ and sapphire.

Our SE results show the energy gap (E_g) of VO₂ to decrease rapidly with heating beginning at temperatures below T_{onset}

(T_{MIT}), the temperature at which ρ decreases faster than the exponential drop characteristic of the low-temperature range.²⁴ The results show that the band gap collapses at $T < T_{\text{MIT}}$, followed by the expected increase in carrier concentration as seen from the plasma frequency (ω_p). The range between T_{onset} and T_{MIT} is pronounced for sample *c*. Raman measurements exhibit diverse temperature dependence for V-O related vibrations, which we attribute to internal stresses in the residual M_1 material as surrounding VO₂ transforms to the high- T phase.

II. EXPERIMENTAL DETAILS

Physical deposition of the VO₂ layers was performed on each substrate using sputtering under identical conditions, details have been previously published.²² SE measurements were carried out between photon energies of 0.6 and 6.5 eV at 70° angle of incidence using the approach detailed by Majumdar *et al.*²⁵ Results were modeled using commercial software. Raman measurements were done in the direct backscattering configuration with 514.5 nm laser excitation kept at low power (<math><10\text{ mW}</math>). In each set of measurements, the sample temperature was varied using a controlled Peltier heater and measured using a calibrated thermistor with values reported within $\pm 0.5^\circ\text{C}$.

A three-layer model is used to simulate the dielectric function of our materials for fitting the measured SE data. The sapphire layer utilizes measurements obtained directly from identical bare substrates oriented in-plane the same as during the VO₂ SE measurements. The second layer is the ~ 120 nm thick VO₂ which we describe using a frequency (ω) dependent, complex dielectric function

$$\varepsilon(\omega) = \varepsilon_\infty + \sum_j \varepsilon_{\text{TL},j}(\omega) + \varepsilon_D(\omega), \quad (1)$$

where ε_∞ is the high-frequency dielectric constant. The model dielectric function in Eq. (1) is taken to be isotropic due to the polycrystalline morphology of our VO₂. The imaginary part of the Tauc-Lorentz (TL) dielectric function in Eq. (1) is

$$\varepsilon_{\text{TL}}^{\text{im}}(\omega) = \begin{cases} \frac{1}{\hbar\omega} \frac{A_j E_{0j} C_j (\hbar\omega - E_g)^2}{\{[(\hbar\omega)^2 - E_{0j}^2]\}^2 + C_j^2 (\hbar\omega)^2}, & E > E_g, \\ 0, & E \leq E_g, \end{cases} \quad (2a)$$

and the real part is obtained from the Cauchy integral

$$\varepsilon_{\text{TL}}^{\text{re}}(\omega) = \frac{2}{\pi} P \int_{E_g}^{\infty} \frac{\xi \varepsilon_{\text{TL}}^{\text{im}}(\xi)}{\xi^2 - (\hbar\omega)^2} d\xi. \quad (2b)$$

The amplitude is A_j , transition energy is E_{0j} , and broadening parameter is C_j .²⁶ The imaginary part of $\varepsilon_{\text{TL},j}(\omega)$ is nonzero in the range where the material absorbs light, $\hbar\omega > E_g$, which generally accounts for band-tail states to define the lowest optical transition. One possible interpretation of the band tail is indirect transitions, as described in Ref. 27 and discussed below. $\varepsilon_D(\omega)$ is the Drude dielectric function

$$\varepsilon_D(\omega) = \frac{\omega_p^2}{-\omega^2 + i\Gamma_D\omega}, \quad (3)$$

with parameters plasma frequency ω_p and broadening factor Γ_D . This term describes the presence of free carriers arising from unintentional doping ($T < T_{\text{MIT}}$)²⁸ and due to the metallic phase ($T > T_{\text{MIT}}$). As expected, the Drude contribution is

small below T_{onset} and grows as the VO₂ becomes metallic above T_{MIT} . The third layer describes the rough (~ 7 nm thick) VO₂ surface, and is modeled using an effective medium approximation consisting of voids intermixed with VO₂. The VO₂ parameters are held the same as for the primary layer with no lateral size and shape dependence taken into account. We also investigated alternatives to the TL function. In particular, we attempted using a series of Lorentzian oscillators. However, these attempts resulted in unsatisfactory fits to our data and so we focus on discussions of the TL approach as in Ref. 18.

III. E_g AND E_{0j} TRANSITIONS BELOW AND ABOVE THE PHASE TRANSITION

Figures 1(a) and 1(b) show, respectively, $\langle\varepsilon_1\rangle$ and $\langle\varepsilon_2\rangle$, the real and imaginary pseudodielectric function of VO₂ for sample *c* at temperatures below T_{onset} , in the intermediate range, and above T_{MIT} . The corresponding results for samples *m* and *r* are shown in Figs. 1(c), 1(d), 1(e), and 1(f), respectively. Below (above) the narrow temperature range shown, the spectra are consistent with those illustrated here for the M_1 (R) phase of VO₂. The imaginary part of dielectric function $\langle\varepsilon_2\rangle$ in each sample increases dramatically at energies below ~ 1.5 eV when each sample reaches T_{MIT} signaling transition to the metallic R phase. Shown in Fig. 1 are the transition energies E_{0j} of the TL oscillators for the low- T M_1 phase (solid lines) and in the R phase above the phase transition (dashed lines). In the following we denote these transitions by unprimed (M_1) and primed (R) integers.

Figure 2 summarizes the experimental results for E_g as a function of T for each sample. In Fig. 3 we show the temperature dependence of the E_{0j} values for each sample. At room temperature our measurements result in E_g values of 0.55, 0.44, and 0.44 eV for samples *c*, *m*, and *r*, respectively. These values are lower than the commonly accepted E_g of 0.6 eV, but fall within the 0.3 to 0.6 eV range of results reported in the literature for bulk samples and material deposited on *c*-sapphire.^{2,3,29,30} Liu *et al.* have calculated the electronic band structure of VO₂ in the M_1 phase.²⁷ They point out that the energy gap may be indirect, arising from transitions between valence states near the B point in the Brillouin zone to conduction levels near the D -symmetry point. The calculated band structure reported by Eyert³¹ also indicates that the energy gap is indirect.

Although the calculated E_g values^{27,31} differ substantially from each other and with our measured results, the possibility that the TL gap from our SE studies may correspond to the weak absorption by indirect transitions is supported by the effect of stress. We correlate variations observed in the room-temperature values obtained for E_g in our samples with the effects of substrate-induced strain characterized along the V-V chains in the metallic rutile phase of VO₂. As discussed above, the C_R axis in sample *c* is under tensile strain, while the C_R -axis lattice constant is compressively strained for samples *m* and *r*. These strains are expected to give rise to blue (tensile) and red (compressive) shifts of the observed optical energy gaps,²⁹ consistent with our observations for E_g . Since indirect energy gaps generally red shift with hydrostatic compression, our results support the interpretation that VO₂ is an indirect gap material in the M_1 phase.

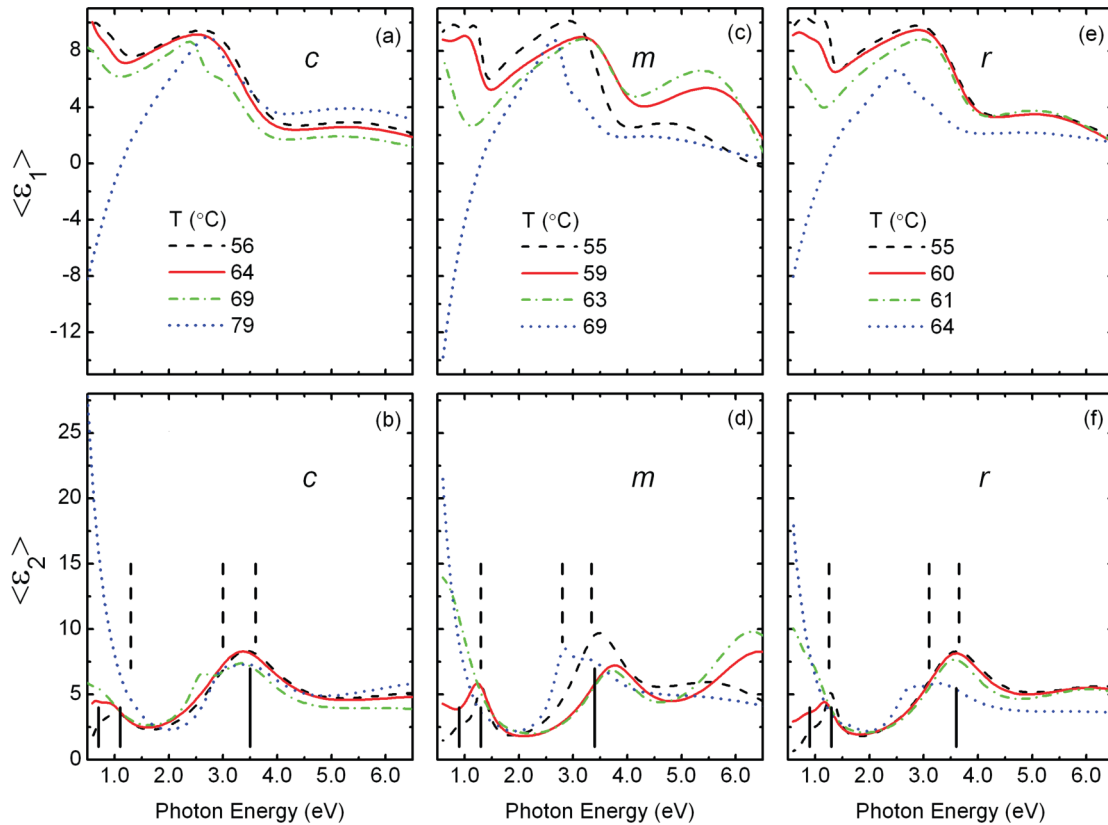


FIG. 1. (Color online) Real $\langle \epsilon_1 \rangle$ and imaginary $\langle \epsilon_2 \rangle$ part of pseudodielectric function of VO₂ at selected temperatures for samples (a) and (b) *c*, (c) and (d) *m*, and (e) and (f) *r*. Solid and dashed lines in the $\langle \epsilon_2 \rangle$ panels demarcate optical transitions in insulating and metallic phases of VO₂, respectively.

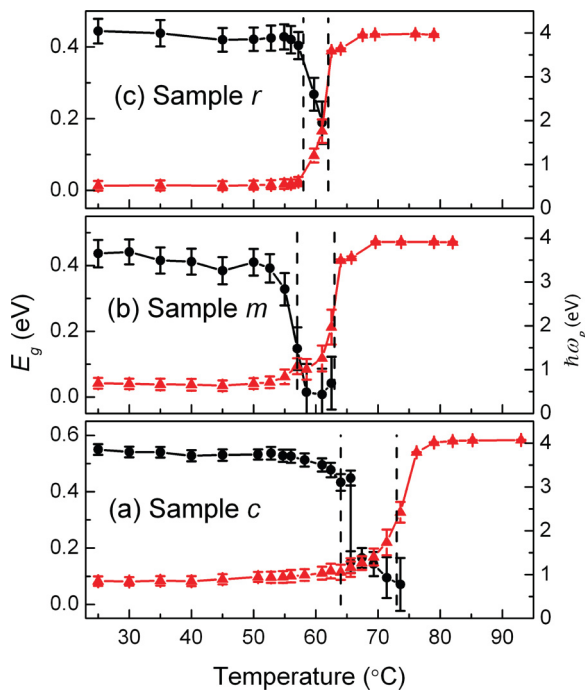


FIG. 2. (Color online) Energy gap (black) and Drude energy (red) as a function of temperature for sample (a) *c*, (b) *m*, and (c) *r*. Vertical dashed lines in each panel represent T_{onset} and T_{MIT} .

Published spectra related to the dielectric function of VO₂ (e.g., $\langle \epsilon \rangle$, index of refraction, and optical conductivity) show overall qualitative agreement, although there remain inconsistencies in the optical transition energies. At room temperature we obtain transition energies E_{0j} at ~ 0.7 , 1.1, and 3.5 eV for sample *c*. These are to be compared with transitions reported 1.4 and 3.2 eV¹⁸ and 1.4 and 3.5 eV²¹ based on spectroscopic ellipsometry. We do not confirm the weak transition reported at 2.5 eV.² As many as five to six features are seen in the optical conductivity of VO₂/TiO₂.²⁰ It is possible that these discrepancies in the literature and with our data are related to the VO₂ growth conditions. However, direct comparison of samples grown under a variety of conditions is needed to examine these discrepancies, and the influence of substrate is critical as we describe here for identical VO₂ preparation on the same substrate material. In samples *m* and *r*, transitions 1 and 2 are shifted by +0.2 eV in comparison to those of sample *c*. These shifts are attributable to strains. Compression results in a blue shift (*m* and *r*), while tension produces a red shift (*c*), as is generally the case for direct transitions in semiconductors. Temperature dependence of the E_{0j} transitions for each sample are summarized in Fig. 3. Transitions are labeled 1(1'), 2(2'), and 3(3'), respectively, below (above) T_{MIT} .³²

Energy levels in VO₂ are commonly interpreted based on the V⁴⁺ ion 3*d* orbitals.³³ In the *M*₁ phase, the bonding

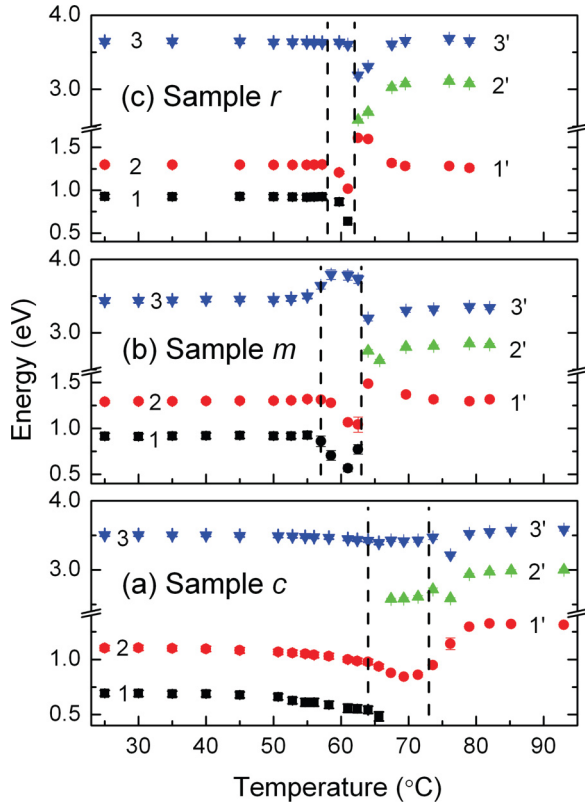


FIG. 3. (Color online) Temperature-dependent optical transitions in semiconductor phase (1, 2, and 3), intermediate and metallic phase (1', 2', and 3') of VO₂ samples (a) *c*, (b) *m*, and (c) *r* obtained from SE measurement. Vertical dashed lines in each panel indicate T_{onset} and T_{MIT} .

d_{\parallel} levels comprise the valence band maxima. These levels are predominantly filled for *n*-type or intrinsic VO₂. Above these states lie the π^* and antibonding d_{\parallel} (denoted d_{\parallel}^*) conduction levels of the 3*d* electrons. The model is illustrated in Fig. 4 at temperatures below T_{onset} (a), $T \sim T_{\text{onset}}$ (b), and above T_{MIT} (c). We assign features 1 and 2 from the ellipsometry measurements to transitions between the filled d_{\parallel} valence levels and empty conduction d states. Feature 3 may be attributed to transitions between the deeper O_{2*p*} levels and

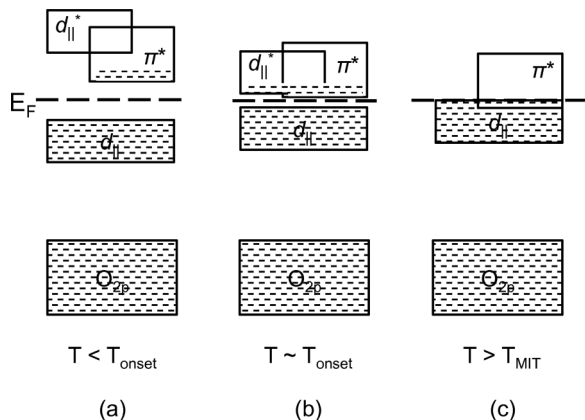


FIG. 4. Band diagram of VO₂ for (a) $T < T_{\text{onset}}$ in insulating phase, (b) intermediated phase at $T \sim T_{\text{onset}}$, and (c) metallic phase at $T > T_{\text{MIT}}$.

the empty π^* bands. In Fig. 4(a) we depict the corresponding band structure for VO₂ well below the phase transition. Since the electronic states in the VO₂ crystal will form bands, it is appropriate to compare our measurements with the results of band structure calculations reported for the monoclinic crystal structure.^{27,29,31,34} Eyert reported density of states (DOS) originating from the O_{2*p*} and 3*d* electrons of VO₂ based on density functional theory (DFT).^{31,34} The high DOS $d_{\parallel} \rightarrow \pi^*$, $d_{\parallel} \rightarrow d_{\parallel}^*$, and O_{2*p*} $\rightarrow \pi^*$ transitions have energies ~ 0.8 , 1.5, and 3.6 eV, respectively, in good agreement with our values for oscillators 1, 2, and 3. Similarly, Lazarovits *et al.*²⁹ carried out local density approximation (LDA) calculations. Based on their spectroscopically resolved DOS results, we estimate the $d_{\parallel} \rightarrow \pi^*$ transition, with high DOS, to have energy ~ 1 eV, while for $d_{\parallel} \rightarrow d_{\parallel}^*$ we estimate ~ 1.5 eV. These are likewise in good agreement with our transitions 1 and 2. Liu *et al.* report band structures without specifically identifying the parent *d*-electron orbitals. From their results, based on DFT, we identify direct transitions at energies ~ 0.9 and 1.1 eV originating from the Γ point in the Brillouin zone of *M*₁-phase VO₂, although it is possible that direct transitions at the *B*-symmetry point contribute near 0.9 eV.²⁷ Again these energies are in reasonable agreement with our transitions 1 and 2. The band structure has multiple bands corresponding to transition 3; therefore we do not give a specific symmetry assignment here.

At $T > T_{\text{MIT}}$ we also observe three bands in this range. These transitions are consistently in the 1.3 eV (1'), 2.8–3.1 eV (2'), and 3.3–3.6 eV (3') ranges. It is plausible that variations in these $E_{0,j}$ values originate from different strains present in the VO₂ above T_{MIT} . Figure 4(c) shows the energy level diagram for the 3*d* and O_{2*p*} electrons in the metallic rutile phase.³³ Oscillator 1' may arise from transitions between d_{\parallel} levels just below the Fermi level (E_F) and π^* states. Comparing this with the calculated band structure,³⁴ we find a good association with the high DOS feature at ~ 1.4 eV. The 2' and 3' bands may be attributed to transitions from the filled O_{2*p*} orbital to the partially filled d_{\parallel} and π^* , respectively.¹⁸ From Ref. 31 we find high DOS transitions from the O_{2*p*} to the E_F at 3.0 eV, as well as O_{2*p*} to multiple high DOS states, with the highest at energy ~ 3.8 eV. Oscillators 1', 2', and 3' correspond to direct transitions between the valence band near E_F to conduction states near the respective *M*, $\bar{}$, and *R* points of the Brillouin zone.³⁴

Upon reaching the metallic phase, the plasma frequency abruptly increases. Energy $\hbar\omega_p$, shown in Fig. 2, begins to rise at temperature T_{onset} , and continues to rise before leveling off above T_{MIT} . Vertical dashed lines in each panel of Figs. 2 and 3 indicate T_{onset} and T_{MIT} . In all samples we obtain $\hbar\omega_p$ of ~ 4.0 eV in the metallic phase. The broadening factor changes slightly from the room-temperature value of 0.85 to 0.73 eV above the phase transition temperature, in agreement with what has been reported for VO₂ deposited on *c*-sapphire.² Cooling reverses the trend (not shown) with the expected hysteresis seen in other measurements. Values obtained for T_{MIT} are 72 ± 2 , 63 ± 2 , and 62 ± 2 °C, for samples *c*, *m*, and *r*, respectively.

IV. TEMPERATURE DEPENDENCE ACROSS THE PHASE TRANSITION

The temperature dependence of E_g is summarized in Fig. 2 for all three samples. A weak overall red shift is observed

until near T_{onset} , where we see a systematic decrease in E_g . At T_{MIT} the value of E_g increases abruptly to ~ 1.1 eV in each sample, although this no longer corresponds to the energy gap in the metallic state. The temperature at which this jump takes place correlates with T_{MIT} based on the ω_P dependence and ρ measurements.²² These changes in the optical properties near T_{onset} and T_{MIT} are also observed in the other bands obtained from our SE measurements, as seen in Fig. 3.

For each sample, T_{onset} agrees with the temperature at which ρ begins to drop more rapidly than the characteristic exponential behavior seen below the phase transition.²² For sample *m* we observe a temperature range below T_{MIT} over which $E_g \sim 0$ eV. This dependence shows that the collapse of the energy gap is gradual and that E_g is close to zero before the MIT. The energy gap also drops at T_{onset} for sample *r*, but because the transition is more abrupt the material becomes metallic without E_g reaching zero. For samples *m* and *r* we depict this situation in Fig. 4(b), for T just below the onset temperature. With E_g near $k_B T$, electrons are activated into the conduction band, giving rise to the observed increase in ω_P below T_{MIT} .

The temperature dependence of E_g for sample *c* is more complex, dropping abruptly at T_{onset} to approximately 0.2 eV, followed by a gradual decrease. However, E_g does not appear to reach zero even very close to T_{MIT} . Our results are consistent with the formation of an intermediate phase between T_{onset} and T_{MIT} , particularly for sample *c*. However, the SE results do not permit us to definitively identify the intermediate phase. One possible interpretation of the phase transformation properties obtained for sample *c* is the presence of a mixed phase consisting of M_1 and R in the intermediate temperature range between T_{onset} and T_{MIT} . This possibility has been suggested by several authors to describe sluggishness in the transition, particularly for thin films.^{35–38} A second possibility is the transformation from M_1 into M_2 VO₂, particularly for sample *c* due to tensile strain along the C_R axis.⁹ Finally, a recent interpretation of the formation of intermediate phase is the triclinic VO₂, which exhibits a gradual transition.¹²

To examine the effect of these transformations on microstructure, we conducted Raman measurements as a function of temperature. Figure 5 shows Raman spectra at various temperatures for each sample, with particular attention to temperatures near the phase transition. Features measured in the Raman spectrum of M_1 -phase VO₂ agree with previously published work.^{39,40} At room temperature, phonon energies for VO₂ depend on substrate orientation, as can be seen in Fig. 6. These differences are most pronounced for the V-O band near 615 cm⁻¹, with phonon energy ascending in order $m \rightarrow r \rightarrow c$. The blue shift is attributable to the tensile stress parallel to the sapphire substrate plane, which produces compressive strain in the growth direction. This same ordering for the vibration near 262 cm⁻¹ suggests a phenomenological association between this feature and the 615 cm⁻¹ V-O vibration. In contrast, strain has a weaker effect on the other Raman bands which exhibit a different ordering at room temperature. This is most notable in the band at 309 cm⁻¹, with energy in ascending order $c \rightarrow r \rightarrow m$. We likewise attribute the observed ordering of the 309 cm⁻¹ band to the different strains in the samples. The tensile strain along the C_R direction in sample *c* will cause the V-V vibrations to red shift, as seen in Fig. 6 from

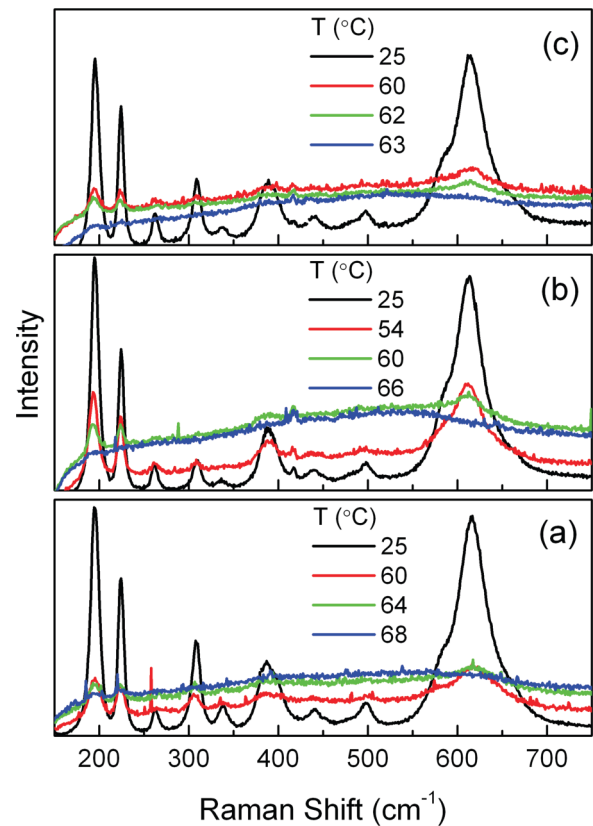


FIG. 5. (Color online) Raman spectra of sample (a) *c*, (b) *m*, and (c) *r* low temperature and near T_{onset} .

comparison of the 309 cm⁻¹ band for the three samples at room temperature.

With increasing temperature, the intensity of the Raman spectrum decreases until near T_{onset} , above which the intensity becomes too weak to detect, as seen in Fig. 5. The temperature dependence of these phonons also differ substantially, as shown in Fig. 6. Each band, including those at ~ 195 , 224, and 309 cm⁻¹, gradually red shifts until becoming too weak to observe. In contrast, the lines near 262 and 615 cm⁻¹ exhibit *diverse* behaviors as T_{onset} is approached. For sample *c*, which has the highest transition temperature, we observe a gradual blue shift followed by a more rapid rise in energy above ~ 55 °C. A gradual blue shift has been recently reported for this Raman band when tensile stress is applied along the C_R direction as VO₂ transforms from M_1 to M_2 at room temperature.¹² However, they also observe the vibrations at ~ 195 and 224 cm⁻¹ to blue shift, contrary to what is seen in Fig. 6(a). This discrepancy indicates that strain induced by mismatches in thermal expansion coefficients is not the sole factor in the temperature dependence of the vibrational structure. For sample *m* the 262 and 615 cm⁻¹ V-O vibrations gradually red shift and then rapidly drop in energy beginning at ~ 55 °C. In sample *r*, with abrupt phase transition, these bands show weak temperature dependence with only a slight red shift just below T_{onset} .

One plausible explanation for the observed trends is the effect of internal stresses in the M_1 -phase VO₂ during the phase transition. These are produced by the neighboring regions which have transformed in the intermediate

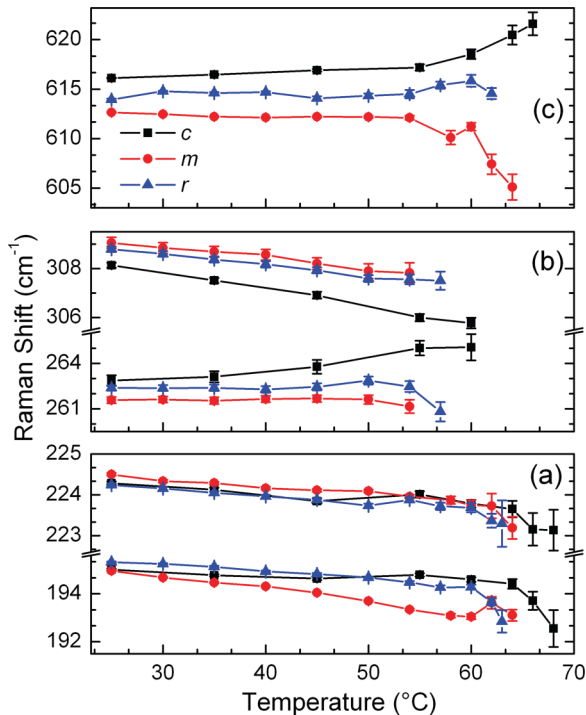


FIG. 6. (Color online) Phonon energies as a function of temperature for peaks at (a) 195 and 225 cm^{-1} , (b) 263 and 309 cm^{-1} , and (c) 615 cm^{-1} .

temperature range. The M_2 phase of VO_2 , for example, expands $\sim 0.8\%$ along the C_R axis.¹³ Partial transformation from M_1 to M_2 would produce compressive stress on the untransformed regions of M_1 -phase VO_2 . This internal stress will increase with transformed volume fraction to steadily blue shift the V-O vibrations with increasing M_2 volume fraction. Using the Young's modulus for VO_2 ⁴¹ and pressure dependence of the 615 cm^{-1} phonon,⁴² we estimate a blue shift of 4 to 6 cm^{-1} , consistent with our observations. For the case where VO_2 transforms directly from M_1 phase into R , the contraction along the C_R axis is expected to red shift the

V-O vibrations. This agrees with what is observed for sample m . Because the known pressure coefficients of the other vibrations (195 and 224 cm^{-1}) are very weak, the impact of internal strains is not substantial. Furthermore, the stress induced by thermal expansion mismatch with the substrate is nearly one order of magnitude smaller than the internal stresses, and are not expected to play a large role in the observed trends in Fig. 6.

V. SUMMARY

We describe diverse phase transformation properties, depending on the VO_2 orientation on c -, m -, and r -plane sapphire. The transformation temperatures T_{onset} and T_{MIT} are related to substrate-induced strains along the C_R crystal axis. We identify three primary, direct optical transitions in both the M_1 and R phases. These are related to energy levels proposed by Goodenough³³ and consistent with recent calculations of the band structure.^{27,29,31,34} For samples m and r , compressive strain along the C_R axis reduces T_{MIT} and results in transformation from M_1 to R -phase VO_2 . An abrupt transition is observed in sample r , while sample m exhibits a more gradual transformation. This may be attributed to the presence of grains having various sizes.^{4,5} For the latter, we observe a temperature range between T_{onset} and T_{MIT} over which the energy gap collapses. Our results are consistent with an indirect energy gap for the M_1 phase of VO_2 , as has been suggested based on band structure calculations.²⁷ In sample c the range between T_{onset} and T_{MIT} is large, consistent with the formation of an intermediate phase of VO_2 . In this case, the energy gap does not completely collapse, remaining in the 0.2 to 0.1 eV range across the phase transition. The effects of internal stresses within partially transformed VO_2 are used to interpret the Raman measurements.

ACKNOWLEDGMENT

The authors acknowledge support for this work from the US National Science Foundation under award ECCS-1128644.

¹F. J. Morin, *Phys. Rev. Lett.* **3**, 34 (1959).

²H. W. Verleur, A. S. Barker, Jr., and C. N. Berglund, *Phys. Rev.* **172**, 788 (1968).

³C. N. Berglund and H. J. Guggenheim, *Phys. Rev.* **185**, 1022 (1969).

⁴R. Lopez, T. E. Haynes, L. A. Boatner, L. C. Feldman, and R. F. Haglund, Jr., *Phys. Rev. B* **65**, 224113 (2002).

⁵D. Brassard, S. Fourmaux, M. Jean-Jacques, J. C. Kieffer, and M. A. El Khakani, *Appl. Phys. Lett.* **87**, 051910 (2005).

⁶Y. Muraoka and Z. Hiroi, *Appl. Phys. Lett.* **80**, 583 (2002).

⁷J. Wu, Q. Gu, B. S. Guiton, N. P. de Leon, L. Ouyang, and H. Park, *Nano Lett.* **6**, 2313 (2006).

⁸J. I. Sohn, H. J. Joo, D. Ahn, H. H. Lee, A. E. Porter, K. Kim, D. J. Kang, and M. E. Welland, *Nano Lett.* **9**, 3392 (2009).

⁹J. Cao, Y. Gu, W. Fan, L. Q. Chen, D. F. Ogletree, K. Chen, N. Tamura, M. Kunz, C. Barrett, J. Seidel, and J. Wu, *Nano Lett.* **10**, 2667 (2010).

¹⁰A. C. Jones, S. Berweger, J. Wei, D. Cobden, and M. B. Raschke, *Nano Lett.* **10**, 1574 (2010).

¹¹Y. Gu, J. Cao, J. Wu, and L.-Q. Chen, *J. Appl. Phys.* **108**, 083517 (2010).

¹²J. M. Atkin, S. Berweger, E. K. Chavez, M. B. Raschke, J. Cao, W. Fan, and J. Wu, *Phys. Rev. B* **85**, 020101 (2012).

¹³M. Marezio, D. B. McWhan, J. P. Remeika, and P. D. Dernier, *Phys. Rev. B* **5**, 2541 (1972).

¹⁴J. P. Pouget, H. Launois, J. P. D'Haenens, P. Merenda, and T. M. Rice, *Phys. Rev. Lett.* **35**, 873 (1975).

¹⁵T. M. Rice, H. Launois, and J. P. Pouget, *Phys. Rev. Lett.* **73**, 3042 (1994).

¹⁶A. Tselev, I. A. Luk'yanchuk, I. N. Ivanov, J. D. Budai, J. Z. Tischler, E. Strelcov, A. Kolmakov, and S. V. Kalinin, *Nano Lett.* **10**, 4409 (2010).

- ¹⁷Y. Cui and S. Ramanathan, *J. Vac. Sci. Technol. A* **29**, 041502 (2011).
- ¹⁸M. M. Qazilbash, A. A. Schafgans, K. S. Burch, S. J. Yun, B. G. Chae, B. J. Kim, H. T. Kim, and D. N. Basov, *Phys. Rev. B* **77**, 115121 (2008).
- ¹⁹J. B. Kana Kana, J. M. Ndjaka, G. Vignaud, A. Gibaud, and M. Maaza, *Opt. Commun.* **284**, 807 (2011).
- ²⁰K. Okazaki, S. Sugai, Y. Muraoka, and Z. Hiroi, *Phys. Rev. B* **73**, 165116 (2006).
- ²¹K. Hiroshi, J. Ping, N. Setsuo, and T. Masato, *Jpn. J. Appl. Phys.* **46**, L113 (2007).
- ²²Y. Zhao, J. H. Lee, Y. Zhu, M. Nazari, C. Chen, H. Wang, A. Bernussi, M. Holtz, and Z. Fan, *J. Appl. Phys.* **111**, 053533 (2012).
- ²³D. Kucharczyk and T. Niklewski, *J. Appl. Crystallogr.* **12**, 370 (1979).
- ²⁴M. Nazari, C. Chen, A. A. Bernussi, Z. Y. Fan, and M. Holtz, *Appl. Phys. Lett.* **99**, 071902 (2011).
- ²⁵A. Majumdar, R. D. Bogdanowicz, and R. Hippler, *Photon. Lett. Poland* **3**, 70 (2011).
- ²⁶J. G. E. Jellison and F. A. Modine, *Appl. Phys. Lett.* **69**, 371 (1996).
- ²⁷G.-H. Liu, X.-Y. Deng, and R. Wen, *J. Mater. Sci.* **45**, 3270 (2010).
- ²⁸C. Chen, Y. Zhao, X. Pan, V. Kuryatkov, A. Bernussi, M. Holtz, and Z. Fan, *J. Appl. Phys.* **110**, 023707 (2011).
- ²⁹B. Lazarovits, K. Kim, K. Haule, and G. Kotliar, *Phys. Rev. B* **81**, 115117 (2010).
- ³⁰C. Blaauw, F. Leenhouts, F. van der Woude, and G. A. Sawatzky, *J. Phys. C* **8**, 450 (1975).
- ³¹V. Eyert, *Phys. Rev. Lett.* **107**, 016401 (2011).
- ³²A fourth broad TL band near 8 eV is required to adequately fit our data for all samples, both below and above the phase transition.
- ³³J. B. Goodenough, *J. Solid State Chem.* **3**, 490 (1971).
- ³⁴V. Eyert, *Ann. Phys.* **11**, 650 (2002).
- ³⁵H.-T. Kim, B.-J. Kim, Y. W. Lee, B.-G. Chae, S. J. Yun, and K.-Y. Kang, *Physica C* **460–462**, 1076 (2007).
- ³⁶J. Cao, E. Ertekin, V. Srinivasan, W. Fan, S. Huang, H. Zheng, J. W. L. Yim, D. R. Khanal, D. F. Ogletree, J. C. Grossman, and J. Wu, *Nat. Nano* **4**, 732 (2009).
- ³⁷M. M. Qazilbash, M. Brehm, G. O. Andreev, A. Frenzel, P. C. Ho, B.-G. Chae, B.-J. Kim, S. J. Yun, H.-T. Kim, A. V. Balatsky, O. G. Shpyrko, M. B. Maple, F. Keilmann, and D. N. Basov, *Phys. Rev. B* **79**, 075107 (2009).
- ³⁸B.-J. Kim, Y. W. Lee, S. Choi, J.-W. Lim, S. J. Yun, H.-T. Kim, T.-J. Shin, and H.-S. Yun, *Phys. Rev. B* **77**, 235401 (2008).
- ³⁹P. Schilbe, *Physica B* **316–317**, 600 (2002).
- ⁴⁰G. I. Petrov, V. V. Yakovlev, and J. Squier, *Appl. Phys. Lett.* **81**, 1023 (2002).
- ⁴¹N. Sepulveda, A. Rua, R. Cabrera, and F. Fernandez, *Appl. Phys. Lett.* **92**, 191913 (2008).
- ⁴²C. Marini, E. Arcangeletti, D. Di Castro, L. Baldassare, A. Perucchi, S. Lupi, L. Malavasi, L. Boeri, E. Pomjakushina, K. Conder, and P. Postorino, *Phys. Rev. B* **77**, 235111 (2008).